Molecular quadrupole moments promote ground-state charge generation in doped organic semiconductors

Alberto Privitera,[±] *Giacomo Londi,*[±] *Moritz Riede, Gabriele D'Avino, David Beljonne*[*]

[±]These authors contributed equally

Dr. Alberto Privitera, Prof. Moritz Riede
Clarendon Laboratory, Department of Physics, University of Oxford, Oxford OX1 3PU, UK

Giacomo Londi, Prof. David Beljonne
Laboratory for Chemistry of Novel Materials, University of Mons, B-7000 Mons, Belgium
E-mail: david.beljonne@umons.ac.be

Dr. Gabriele D'Avino
Institut Néel, CNRS and Grenoble Alpes University, F-38042 Grenoble, France

Keywords: Molecular doping, charge generation, quadrupole moment, organic semiconductors

Abstract

The role of local environmental interactions on the generation of free charge carriers in doped organic layers is investigated. Via a classical micro-electrostatic model, a dual effect of molecular quadrupole moments of host and dopant molecules on doping is demonstrated. Namely, electrostatic interactions ease ionization of the dopant by altering the energy level alignment between the host and the dopant and reduce the barrier for charge dissociation by flattening the energy landscape around the ionized dopants. These results indicate that tailoring molecular quadrupole moments of the host and/or dopant is an attractive strategy towards improved doping efficiency in organic semiconductors.

1. Introduction

Molecular doping has proven to be a game-changer in the field of organic optoelectronics as it allows for example the precise alignment of the energy levels at the interfaces of multi-layer devices and the minimization of Ohmic losses at the electrodes.[1] As a result, molecular doping has laid the foundations for the development of efficient organic devices including organic light emitting diodes (OLEDs), organic field effect transistors (OFETs) and organic solar cells (OSCs).[2] The last years witnessed a considerable advancement of the research on doped organic semiconductors.[3] These efforts led to a better understanding of the relationships between structure and properties in doped materials,[4a] as well as to the emergence of novel strategies to dope organic semiconductors, including light-activated dopants,[4b] anion exchange processing,[4c] and the emergence of Lewis acids complexes as molecular dopants.[4d]

Recent studies have shown that the charge generation in doped organic semiconductors consists of two elementary steps.[1b, 4-5] The first step involves either a hybridization of the host-dopant frontier molecular orbitals or a ground-state integer charge transfer (CT) process between the host and the dopant.[1a, 6] For p-type doping, the latter is favoured when the energy difference between the ionization potential (IP) of the host and the electron affinity (EA) of the dopant (i.e. the host-dopant gap $\Gamma_{hd} = IP_{host} - EA_{dop}$) is smaller in magnitude than the Coulomb binding energy between an electron and its geminate hole sitting on nearest neighbour molecules (V_{eh}).[7] In such conditions, a *bound* CT state with an electron added to the dopant and a hole left on the host molecule is generated.[11,12] This is the ionization step. The second step, namely the charge dissociation, then consists of the spatial migration of the hole (for p-doping) away from the ionized acceptor that requires overcoming the large Coulomb binding of the CT pair, which usually amounts to several hundreds of meV.[4a,8] The energetic and kinetic aspects of both steps need to be concomitantly optimized in order to maximize the overall charge generation efficiency, which calls for a control of the interactions between the molecules at the microscopic level.[3]

Tuning these microscopic interactions can be achieved by molecular and material engineering. For instance, *Warren et al.* demonstrated that the energy levels in an organic semiconductor and the Fermi energy can be simultaneously tuned by taking advantage of molecular quadrupolar interactions.[1c] This result was achieved by co-evaporating a host mixture between zinc-phthalocyanine (ZnPc) and its eight-times fluorinated counterpart (F_8ZnPc) together with the p-type dopant F6-TCNNQ. Such mixtures are very interesting because they provide an effective and practical approach to finely control the p-doping efficiency of F6-TCNNQ upon tuning the host energy levels, which are a function of the ZnPc:F_8ZnPc molar ratio.[1c, 9]

Here, in the wake of the very recent experimental work reported by *Warren et al.*,[1c] we investigate the role of environmental interactions on the charge generation mechanism in doped binary (ZnPc:F6-TCNNQ and F_8ZnPc:F6-TCNNQ) and ternary (ZnPc:F_8ZnPc:F6-TCNNQ) blends. Based on an in-depth atomistic modelling of electrostatic and dielectric phenomena in molecular solids,[10] we show that charge-quadrupole interactions affect both the ionization step (by reshuffling the energy levels of the dopant and the host) and the charge dissociation step (by creating a favourable energy pathway for the hole). Interestingly, besides long-range electrostatics phenomena characterizing the energy landscape of ordered molecular films,[10] we observe that the substitution of a host molecule with F6-TCNNQ has a significant short-range effect, namely the IP of the host molecules next to a dopant impurity strongly differ (up to 0.4 eV) from the IPs of the other host molecules. This electrostatic contribution is due to the difference in quadrupole moment between F6-TCNNQ and the host molecules, and it significantly affects the host-dopant gap Γ_{hd}, which on average amounts to 0.63 eV for ZnPc and 0.86 eV for F_8ZnPc. When accounting for screened electron-hole Coulomb interactions (V_{eh}~ 0.65 eV for all samples), we find an overall energy barrier that is close to zero for the ionization step in a binary ZnPc:F6-TCNNQ blend. In F_8ZnPc:F6-TCNNQ this barrier is 0.2 eV larger, in line with the poorer ionization efficiency observed in literature for the latter blend. Most interestingly, the explicit calculation of the energy profile for charge separation, reveals

that the quadrupole moments of dopant impurities can positively impact this crucial second step. We believe these results pave the way towards a full control of *both* steps (ionization and charge dissociation) in the doping of organics through the proper engineering of molecular quadrupolar moments.

2. Results

2.1. Binary Blends

First, we calculated the gas-phase IP and EA of the host (ZnPc and F_8ZnPc) and p-dopant (F6-TCNNQ) molecules (see chemical structures in **Figure 1a** and **SI2**) at the ev*GW* many-body perturbation theory level.[11] The obtained values, reported in **Figure SI3**, are in excellent agreement with the experimental ones,[12] and indicate an increase in both the molecular IP and EA by ~0.5 eV upon fluorination, as a result of the strong, inductive, electron-withdrawing effects induced by the fluorine atoms.[13] The huge energy difference in the gas-phase between the EA of F6-TCNNQ (4.44 eV) and the IP of the host (6.41 eV for ZnPc and 6.91 eV for F_8ZnPc) would completely impede ground-state CT. The situation changes dramatically when accounting for environmental solid-state effects on the energy levels of both the host and dopant molecules.[10, 14] In molecular solids, the IP and EA values depend strongly on collective, long-range, electrostatic effects associated with the varying charge density distributions in the neutral and ionized molecules. These include induction effects, describing the dielectric screening of the polarizable medium to an added charge, and electrostatic interactions, brought about by the molecular electrical multipole moments.[10] In our case, electrostatic interactions are led by the quadrupole term, since the molecules of interest are centrosymmetric and have no dipole moment.[9a]

We first consider the case of a F6-TCNNQ dopant as a single substitutional impurity in two pristine lattices, the first made of ZnPc molecules and the second of F_8ZnPc ones. We specifically considered films (2D slab calculations) of the two compounds, composed of molecular stacks whose axes lie in the film plane, leading to an edge-on molecular orientation

with respect to the slab normal (Figure SI4).[9a] This molecular orientation has been proposed from our previous GIWAXS analysis and is in line with literature studies.[1b,1c,9a] Electrostatic and induction phenomena are described here with a classical Micro-Electrostatic (ME) model of atomistic resolution, see Methods in SI.[15] Our calculations reveal large environmental effects on charge energetics, as shown in **Figure 1b** and **1c** and reported on **Table SI2**. In line with earlier findings, we notice that induction interactions reduce the host-dopant gap by ~2 eV irrespective on the host material, as a result of the similar dielectric susceptibilities of organic solids.[10]

On top of induction, the electrostatic contribution further affects the energy levels with an amplitude and sign that depend on the host material. Namely, these interactions are determined by the component of the traceless quadrupolar tensor perpendicular to the molecular plane, which is negative in ZnPc and positive in F_8ZnPc because of the inverted polarity of C-F vs C-H bonds (Figure 1a and Table SI1). In Figure 1b and 1c, we distinguish between the IP of a host molecule in the pristine host material (open circle) and an host molecule next to the dopant along the π stacking axis (full circle), which we consider the most important direction for both charge motion and electrostatic interactions. We notice that the signs of the electrostatic shifts of the energy levels of both the dopant (EA, blue triangle) and of its neighbouring host molecule (IP, full circle) is the same as the pristine host (IP, open circle). Electrostatic shifts are negative in the ZnPc host (Figure 1b) and positive in F_8ZnPc (Figure 1c). This determines a 1 eV difference in the EA of the F6-TCNNQ depending on the host material, in line with recent findings by some of us.[14] Interestingly, we also observe that the levels of host molecules strongly depend on their position with respect to the dopant, being the IP of the molecule near the dopant significantly different (0.3-0.4 eV) from that of a host molecule in the pristine host or at infinite distance from the dopant. The position dependence of the host levels can be ascribed to the quadrupolar interaction with the dopant, characterized by an electrostatic layout that is markedly different from that of the replaced host molecule. As it originates from the

quadrupole of the single dopant molecule, this effect is rather short-ranged and has an appreciable impact only on the nearest-neighbour molecules.

2.2. Ternary Blends

We now turn our attention to the energy levels of ternary blends composed by a mixed ZnPc:F_8ZnPc host, doped with a F6-TCNNQ molecule. ME calculations were carried out for different host mixing ratios, ranging from pure ZnPc to pure F_8ZnPc. For the 1:1 ratio, we opt for an alternating ZnPc:F_8ZnPc mixed-stack motif, which is expected to be the most stable structure for π-stacked molecules with opposite quadrupoles. A similar alternating packing was recently resolved for a 1:1 co-crystal of pentacene and perfluoropentacene.[16] Crystalline supercells of blends with different ratio were created in a similar way but with a different alternating periodicity (one ZnPc molecule every two F_8ZnPc molecules, and vice versa). Our calculations for the energy levels in undoped ZnPc:F_8ZnPc blends of different composition (**Figure SI5**) are in substantial agreement with the similar ones reported by Schwarze e*t al.*[9a] The energy levels of host and dopant molecules in ternary blends are shown in **Figure 2a**. Since different microscopic configurations can be generated upon introducing a dopant in the ZnPc:F_8ZnPc blends (for the 1:1 ratio, the dopant can be placed both at ZnPc and F_8ZnPc site; more configurations are possible for other host compositions), the figure displays the average over the possible microstructures, which is representative of the specific values reported in **Figure SI6**. Calculations in **Figure 2a** show that the energy levels of host molecules and dopant evolve linearly with the ZnPc molar ratio, as all the molecules probe an effective quadrupolar field resulting from the additive contributions sourced by the two host molecules. Most importantly, this translates into a host-dopant gap Γ_{hd} that does not significantly vary with the host mixing ratio, leading to the conclusion that replacing a significant fraction of ZnPc molecules by electron-poor F_8ZnPc should not be overly detrimental to ionization, at least from an energetic point of view. This is an important result that laid down the foundation of the statistical approach successfully used by *Warren et al.* to model the ternary blends.[1c]

On average, when accounting for the whole range of host chemical composition, Γ_{hd} ranges from 0.63 eV for ZnPc to 0.86 eV in F_8ZnPc (Figure 2b). This energy difference is largely compensated by the screened electron-hole Coulomb binding energy V_{eh} (~0.65 eV), making the overall ionization process barrier-free for ZnPc, while still significantly activated (energy barrier ~0.2 eV) for F_8ZnPc (**Figure 2b**). This is in good agreement with the high ionization efficiency experimentally measured in the ZnPc:F6-TCNNQ blends.[1c] Conversely, the energy to ionize the dopant in the F_8ZnPc host remains positive and larger than the thermal energy, which points to a low ionization efficiency, in line with our previous experimental results.[1c] In addition to V_{eh}, we considered the role played by structural reorganization upon charging,[14] quantified by $\lambda = \lambda^+ + \lambda^- \sim 0.15$ eV, being λ^+ and λ^- the hole and electron reorganization energies of dopant and host, respectively. This contribution, which we computed in gas-phase, represents an upper estimate of the relaxation energy in the solid state where molecular geometries are constrained. Structural reorganization further stabilizes the CT state, hence making the ionization step energetically more favourable (Figure 2b). When accounting for this contribution in full (the geometric relaxation might be partly hindered by steric constraints in the solid), the ionization remains considerably more favourable (by ~200 meV) in ZnPc compared to F_8ZnPc. Considering the typical error bar (~100 meV) on the calculated energies and other approximations used in the model (i.e. the neglect of dynamic disorder), a limited electron transfer between the tail states of the dopant and F_8ZnPc molecules cannot be excluded from our simulations, as it could not be ruled out on the basis of our previous EPR data.[1c]

2.3. Charge separation

Moving on further, we discuss the results of ME calculations explicitly targeting the electron-hole separation energy profile along the π stacking direction. **Figure 3** and **Table SI5** report the energies of the CT states and the Coulomb binding energies V_{eh} as a function of the hole distance from the F6-TCNNQ anion for the ZnPc:F6-TCNNQ and F_8ZnPc:F6-TCNNQ binary blends and for ternary blends with 1:1 ZnPc:F_8ZnPc composition, distinguishing the two cases

where the dopant sits at the molecular site of ZnPc or F_8ZnPc. Remarkably, our calculations highlight that the energy barrier for charge separation (E_{cs}) of the CT state is significantly lower than the mere Coulomb binding energy V_{eh} ~ 0.65 eV (compare red and black lines in Figure 3). This is essentially due to the effect of the quadrupolar field of the F6-TCNNQ dopant, that destabilizes CT states with charges localized on neighboring molecules (see **Figure 2**, **Table SI4** and **Figure SI7**). The magnitude of this effect depends however on the host composition and on the dopant location, with E_{cs} ranging from 0.37 eV in F_8ZnPc (**Figure 3b**), down to 0.15 eV in the ZnPc:F_8ZnPc blend when the impurity substitutes a ZnPc molecule (**Figure 3d**). In the latter case, and similarly in ZnPc:F6-TCNNQ (**Figure 3a**), the energy profile for charge separation is rather flat, rationalizing the possibility for a thermally activated charge separation observed for these two systems.[1c] This energy level bending effect sourced by electrostatic intermolecular interactions, similar to those previously reported in the context of photoinduced charge separation at donor-acceptor interfaces,[17] provide a decisive contributions to holes to escape the Coulomb well of their parent dopant.

3. Conclusion

This work delved into the effect of the environmental solid-state interactions on the generation of free charge carriers by doping organic semiconductors. We carried out our investigations on a model system comprising ZnPc:F_8ZnPc blends, as a host, p-doped with F6-TCNNQ. This ternary blend allows to control doping efficiency by simply varying the ZnPc molar ratio.[1c] Our theoretical work disclosed the fundamental role of charge-quadrupolar interactions emerging at different length scales on both (1) the ionization and (2) the charge dissociation steps of molecular doping. Our modelling revealed that the presence of a substitutional F6-TCNNQ molecule in the host lattice strongly influence the IP of the nearest-neighbor molecules without significantly affecting those further apart, ultimately controlling both steps of the doping process. As for the ionization step, this short-range electrostatic contribution significantly increases (up to 0.4 eV) the host-dopant gap. After considering the electron-hole

Coulomb interaction, the energy barrier for the formation of a bound CT state between nearest-neighbour molecules becomes close to zero for ZnPc:F6-TCNNQ and is ~0.2 eV larger for F_8ZnPc:F6-TCNNQ, in line with the larger ionization efficiency measured in the former blend.[1c] The charge dissociation step is expected to be very inefficient on the sole consideration of the Coulomb binding energy of the generated holes to their ionized acceptors, with V_{eh} as large as ~0.65 eV. Remarkably, however, this is largely alleviated by the short-range perturbation of the quadrupole moment of the dopant impurity that, destabilizing CT states between nearest-neighbour molecules, results in a more favourable energy landscape for charge dissociation, with residual effective energy barriers in the range 0.15-0.37 eV depending on the host composition and local micro-structural configuration.

On a more general vein, our findings highlight that the control of electrostatic interactions in thin films is essential to foster both the ionization and the charge dissociation steps in molecular doping. This control requires to simultaneously master the molecular electrostatic moments and the supramolecular organization. Molecular ternary blends of variable composition offer a versatile platform for dissecting the different effects at play, paving the way for the development of new organic semiconductors with improved doping efficiency based on molecular electrostatics engineering.

4. Experimental Section

Gas-phase ground state geometry optimizations were carried out at density functional theory (DFT) level with the Gaussian16[18] suite, using the PBE0 functional and the cc-pVTZ basis set. The point group symmetry (D_{4h} for ZnPc and F_8ZnPc, and C_{2h} for F6-TCNNQ) was retained during the optimizations. Molecular quadrupole moments are defined as

$$Q_{ij} = \int \rho(\boldsymbol{r}) \left(r_i r_j - \frac{1}{3} |\boldsymbol{r}|^2 \delta_{ij} \right) d\boldsymbol{r}$$

where i and j label Cartesian components and $\rho(\boldsymbol{r})$ is the molecular charge density, including nuclei. Gas-phase *GW* calculations were performed starting from Kohn-Sham eigenstates calculated for the optimized molecular structures with the ORCA package.[19] A partial self-

consistent scheme on the eigenvalues (ev*GW*) was used, along with the cc-pVXZ basis set (where X = D, T). Then, quasiparticle energy levels IP_g and EA_g were extrapolated to the complete basis set (CBS) limit.[14] The universal Weigend Coulomb fitting set of functions was used as auxiliary basis in the resolution of identity (RI-V) approach. ev*GW* calculations were performed with the Fiesta package.[11a]

MicroElectrostatic (ME) calculations were parametrized with ESP atomic charges and polarizability tensor calculated with DFT at the PBE0/cc-pVTZ level of theory. ESP charges were computed for all the neutral species, for the positively charged ZnPc and F_8ZnPc and for the negatively charged F6-TCNNQ. The polarizability of charged species was set equal to that of neutral ones. Our ME scheme, implemented in the MESCal code,[15] relies on a point-charge description of the molecular charge distributions and on tensor dipole polarizabilities distributed at atomic sites. The solid-state charge carrier transport levels were calculated as:

$$IP = IP_g + \Delta^h$$

$$EA = EA_g - \Delta^e$$

Environmental solid-state effects entail a polarization and an electrostatic contribution:

$$\Delta^x = \Delta_I^x + \Delta_E^x$$

where *x* labels the charged excitation (electron or hole). The polarization Δ_I^x term describes the dynamical response of the surrounding dielectric medium to the presence of a charge carrier. The electrostatic Δ_E^x term corresponds to the energy to charge a molecule in the electrostatic field of all other molecules in the neutral crystal.[16]

Charge transfer (CT) states with localized charges are modelled as classical electron-hole pairs. The binding energy V_{eh} of ion pairs is computed as the sum of screened Coulomb interactions between a hole residing on a host molecule (ZnPc or a F_8ZnPc) and an electron on the F6-TCNNQ dopant:

$$V_{eh} = \frac{1}{\varepsilon_r} \sum_{i,j} \frac{\delta q_i^e \delta q_j^h}{r_{ij}}$$

where $\varepsilon_r = 3.2$ is the computed dielectric constant of the medium.

The structural relaxation energies $\lambda^{\pm}$ upon charging were computed at the DFT level (PBE0/cc-pVTZ) by comparing the vertical and the adiabatic IP and EA of the hosts and of the dopant, respectively. In F6-TCNNQ the dihedral angles involving the dicyanovinyl groups were kept frozen during the optimizations, in order to get rid of low-frequency contributions to $\lambda = \lambda^+ + \lambda^-$. Specifically, $\lambda^+ = 20\ meV$ for ZnPc, $\lambda^+ = 37\ meV$ for F_8ZnPc and $\lambda^- = 131\ meV$ for F6-TCNNQ.

Molecular stacks were build following the recipe described in Ref.[9a], starting from the crystallographic structure of CuPc,[20] replacing the Cu atoms with Zn ones and replicating the unit cell along the 3 directions. The convergence of the electrostatic energy Δ_E^x was checked with calculations considering pure ZnPc films of 3 (5x17x3 supercell) and 5 (5x17x3 supercell) molecular layers stacked along the film normal direction *z*. Δ_E^x of a central ZnPc molecule in each layer was computed accounting for periodic replica in the *x*-*y* plane within a cut-off distance *R* ranging from 120 to 300 Å. The electrostatics converged (within 20 meV) in the 3 middle layers for a 5x17x5 supercell with a cut-off of 300 Å. Therefore, all subsequent calculations employed a 5x17x3 stack with 300 Å in-place cut-off for the computations of the Δ_E^x terms. On the other hand, polarization energies Δ_I^x were calculated for spherical clusters of increasing radii extracted from the bulk structure and centered at the molecule of interest and extrapolated for an infinite system.

Author contribution

AP and GL conceived and designed the project with significant input from DB, GD and MR. GL and AP carried out all the DFT and ME calculations. DB and GD supervised the work and contributed with fruitful discussion. The first manuscript draft was prepared by AP and GL. All the authors reviewed the manuscript and participated actively in the final discussion of the results.

Supporting Information

Supporting Information is available from the Wiley Online Library or from the author.

Acknowledgements

This work was supported by European Union's Horizon 2020 research and innovation programme under Marie Sklodowska Curie Grant agreement No.722651 (SEPOMO project) and by the EPSRC (EP/L011972/1). Computational resources in Mons were provided by the Consortium des Équipements de Calcul Intensif (CÉCI), funded by the Fonds de la Recherche Scientifiques de Belgique (F.R.S.-FNRS) under Grant No. 2.5020.11, as well as the Tier-1 supercomputer of the Fedération Wallonie-Bruxelles, infrastructure funded by the Walloon Region under Grant Agreement No. 1117545. D.B. is a FNRS Research Director. G.L., G.D. and D.B. gratefully thank Xavier Blase for discussions on many-body perturbation theory and for sharing the FIESTA code.

Received: ((will be filled in by the editorial staff))
Revised: ((will be filled in by the editorial staff))
Published online: ((will be filled in by the editorial staff))

References

[1] a) I. Salzmann, G. Heimel, M. Oehzelt, S. Winkler, N. Koch, *Acc. Chem. Res.* **2016**, 49, 370; b) M. L. Tietze, J. Benduhn, P. Pahner, B. Nell, M. Schwarze, H. Kleemann, M. Krammer, K. Zojer, K. Vandewal, K. Leo, *Nat. Commun.* **2018**, 9, 1182; c) R. Warren, A. Privitera, P. Kaienburg, A. E. Lauritzen, O. Thimm, J. Nelson, M. K. Riede, *Nat. Commun.* **2019**, 10, 5538; d) I. E. Jacobs, A. J. Moule, *Adv. Mater.* **2017**, 29.

[2] a) B. Lussem, C. M. Keum, D. Kasemann, B. Naab, Z. Bao, K. Leo, *Chem. Rev.* **2016**, 116, 13714; b) B. Lüssem M. Riede K. Leo, *phys. stat. sol. (a)* **2013**, 210, 9; c) K. Walzer, B. Maennig, M. Pfeiffer, K. Leo, *Chem. Rev.* **2007**, 107, 1233.

[3] a) S.-J. Wang, D. Venkateshvaran, M. R. Mahani, U. Chopra, E. R. McNellis, R. Di Pietro, S. Schott, A. Wittmann, G. Schweicher, M. Cubukcu, K. Kang, R. Carey, T. J. Wagner, J. N. M. Siebrecht, D. P. G. H. Wong, I. E. Jacobs, R. O. Aboljadayel, A. Ionescu, S. A. Egorov, S. Mueller, O. Zadvorna, P. Skalski, C. Jellett, M. Little, A. Marks, I. McCulloch, J. Wunderlich, J. Sinova, H. Sirringhaus, Nat. Electr. 2019, 2, 98; b) S. Fratini, M. Nikolka, A. Salleo, G. Schweicher, H. Sirringhaus, Nat. Mater. 2020 c) M. Arvind, C. Tait, M. Guerrini, J. Krumland, A. M. Valencia, C. Cocchi, A. E. Mansour, N. Koch, S. Barlow, S. R. Marder, J. Behrends, D. Neher, J. Phys. Chem. B 2020, XXXX, XXX, XXX-XXX d) A. Jha, H. G. Duan, V. Tiwari, M. Thorwart, R. J. D. Miller, Chem. Sci. 2018, 9, 4468. e) K. Xu, H. Sun, T.-P. Ruoko, G. Wang, R. Kroon, N. B. Kolhe, Y. Puttisong, X. Liu, D. Fazzi, K. Shibata, C.-Y. Yang, N. Sun, G. Persson, A. B. Yankovich, E. Olsson, H. Yoshida, W. M. Chen, M. Fahlman, M. Kemerink, S. A. Jenekhe, C. Müller, M. Berggren, S. Fabiano, Nat. Mater. 2020, 19, 738–744.

[4] a) M. Schwarze, C. Gaul, R. Scholz, F. Bussolotti, A. Hofacker, K. S. Schellhammer, B. Nell, B. D. Naab, Z. Bao, D. Spoltore, K. Vandewal, J. Widmer, S. Kera, N. Ueno, F. Ortmann, K. Leo, Nat. Mater. 2019, 18, 242; b) X. Lin, B. Wegner, K. M. Lee, M. A. Fusella, F. Zhang, K. Moudgil, B. P. Rand, S. Barlow, S. R. Marder, N. Koch, A. Kahn, Nat. Mater. 2017, 16, 1209–1215; c) Y. Yamashita, J. Tsurumi, M. Ohno, R. Fujimoto, S. Kumagai, T. Kurosawa, T. Okamoto, J. Takeya, S. Watanabe, Nature 2019, 572, 634–638; d) B. Yurash, D. X. Cao, V. V. Brus, D. Leifert, M. Wang, A. Dixon, M. Seifrid,

A. E. Mansour, D. Lungwitz, T. Liu, P. J. Santiago, K. R. Graham, N. Koch, G. C. Bazan, T.-Q. Nguyen, Nat. Mater. 2019, 18, 1327–1334.

[5] M. L. Tietze, P. Pahner, K. Schmidt, K. Leo, B. Lüssem, *Adv. Funct. Mater.* **2015**, 25, 2701.

[6] a) H. Mendez, G. Heimel, S. Winkler, J. Frisch, A. Opitz, K. Sauer, B. Wegner, M. Oehzelt, C. Rothel, S. Duhm, D. Tobbens, N. Koch, I. Salzmann, *Nat. Commun.* **2015**, 6, 8560; b) I. Salzmann, G. Heimel, S. Duhm, M. Oehzelt, P. Pingel, B. M. George, A. Schnegg, K. Lips, R. P. Blum, A. Vollmer, N. Koch, *Phys. Rev. Lett.* **2012**, 108, 035502.

[7] a) B. Wegner, L. Grubert, C. Dennis, A. Opitz, A. Röttger, Y. Zhang, S. Barlow, S. R. Marder, S. Hecht, K. Müllen, N. Koch, *J. Mater. Chem. C* **2019**, 7, 13839; b) J. Li, G. D'Avino, A. Pershin, D. Jacquemin, I. Duchemin, D. Beljonne, X. Blase, *Phys. Rev. Mater.* **2017**, 1, 025602.

[8] a) J.-M. Kim, S.-J. Yoo, C.-K. Moon, B. Sim, J.-H. Lee, H. Lim, J. W. Kim, J.-J. Kim, *J. Phys. Chem. C* **2016**, 120, 9475; b) J. Li, G. D'Avino, A. Pershin, D. Jacquemin, I. Duchemin, D. Beljonne, X. Blase, *Phys. Rev. Mater.* **2017**, 1.

[9] a) M. Schwarze, W. Tress, B. Beyer, F. Gao, R. Scholz, C. Poelking, K. Ortstein, A. A. Günther, D. Kasemann, D. Andrienko, K. Leo, *Science* **2016**, 352, 1446; b) P. R. Warren, J. F. M. Hardigree, A. E. Lauritzen, J. Nelson, M. Riede, *AIP Adv.* **2019**, 9, 035202.

[10] G. D'Avino, L. Muccioli, F. Castet, C. Poelking, D. Andrienko, Z. G. Soos, J. Cornil, D. Beljonne, *J. Phys.: Condens. Matter* **2016**, 28, 433002.

[11] a) X. Blase, C. Attaccalite, V. Olevano, *Phys. Rev. B* **2011**, 83, 115103; b) J. Li, G. D'Avino, I. Duchemin, D. Beljonne, X. Blase, *Phys. Rev. B* **2018**, 97, 035108.

[12] D. A. da Silva Filho, V. Coropceanu, N. E. Gruhn, P. H. de Oliveira Neto, J.-L. Brédas, *Chem. Commun.* **2013**, 49, 6069.

[13] M. Brendel, S. Krause, A. Steindamm, A. K. Topczak, S. Sundarraj, P. Erk, S. Höhla, N. Fruehauf, N. Koch, J. Pflaum, *Adv. Funct. Mater.* **2015**, 25, 1565.

[14] J. Li, I. Duchemin, O. M. Roscioni, P. Friederich, M. Anderson, E. Da Como, G. Kociok-Köhn, W. Wenzel, C. Zannoni, D. Beljonne, X. Blase, G. D'Avino, *Mater. Horiz.* **2019**, 6, 107.

[15] G. D'Avino, L. Muccioli, C. Zannoni, D. Beljonne, Z. G. Soos, *J. Chem. Theory Comput.* **2014**, 10, 4959.

[16] G. D'Avino, S. Duhm, R. G. Della Valle, G. Heimel, M. Oehzelt, S. Kera, N. Ueno, D. Beljonne, I. Salzmann, *Chem. Mater.* **2020**, 32, 1261.

[17] a) F. Castet, G. D'Avino, L. Muccioli, J. Cornil, D. Beljonne, *PCCP* **2014**, 16, 20279; b) G. D'Avino, S. Mothy, L. Muccioli, C. Zannoni, L. Wang, J. Cornil, D. Beljonne, F. Castet, *J. Phys. Chem. C* **2013**, 117, 12981; c) S. Athanasopoulos, S. Tscheuschner, H. Bässler, A. Köhler, *J. Phys. Chem. Lett.* **2017**, 8, 2093; d) J. Idé, R. Méreau, L. Ducasse, F. Castet, H. Bock, Y. Olivier, J. Cornil, D. Beljonne, G. D'Avino, O. M. Roscioni, L. Muccioli, C. Zannoni, *J. Am. Chem. Soc.* **2014**, 136, 2911.

[18] M. J. Frisch, G. W. Trucks, H. B. Schlegel, G. E. Scuseria, M. A. Robb, J. R. Cheeseman, G. Scalmani, V. Barone, G. A. Petersson, H. Nakatsuji, X. Li, M. Caricato, A. V. Marenich, J. Bloino, B. G. Janesko, R. Gomperts, B. Mennucci, H. P. Hratchian, J. V. Ortiz, A. F. Izmaylov, J. L. Sonnenberg, Williams, F. Ding, F. Lipparini, F. Egidi, J. Goings, B. Peng, A. Petrone, T. Henderson, D. Ranasinghe, V. G. Zakrzewski, J. Gao, N. Rega, G. Zheng, W. Liang, M. Hada, M. Ehara, K. Toyota, R. Fukuda, J. Hasegawa, M. Ishida, T. Nakajima, Y. Honda, O. Kitao, H. Nakai, T. Vreven, K. Throssell, J. A. Montgomery Jr., J. E. Peralta, F. Ogliaro, M. J. Bearpark, J. J. Heyd, E. N. Brothers, K. N. Kudin, V. N. Staroverov, T. A. Keith, R. Kobayashi, J. Normand, K. Raghavachari, A. P. Rendell, J. C. Burant, S. S. Iyengar, J. Tomasi, M.

Cossi, J. M. Millam, M. Klene, C. Adamo, R. Cammi, J. W. Ochterski, R. L. Martin, K. Morokuma, O. Farkas, J. B. Foresman, D. J. Fox, Wallingford, CT 2016.
[19] F. Neese, *WIREs Comput. Mol. Sci.* **2012**, 2, 73.
[20] Y. T. a. H. M. A. Hoshino, *Acta Crystallogr. Sect. B: Struct. Sci.* **2003**, B59, 393.

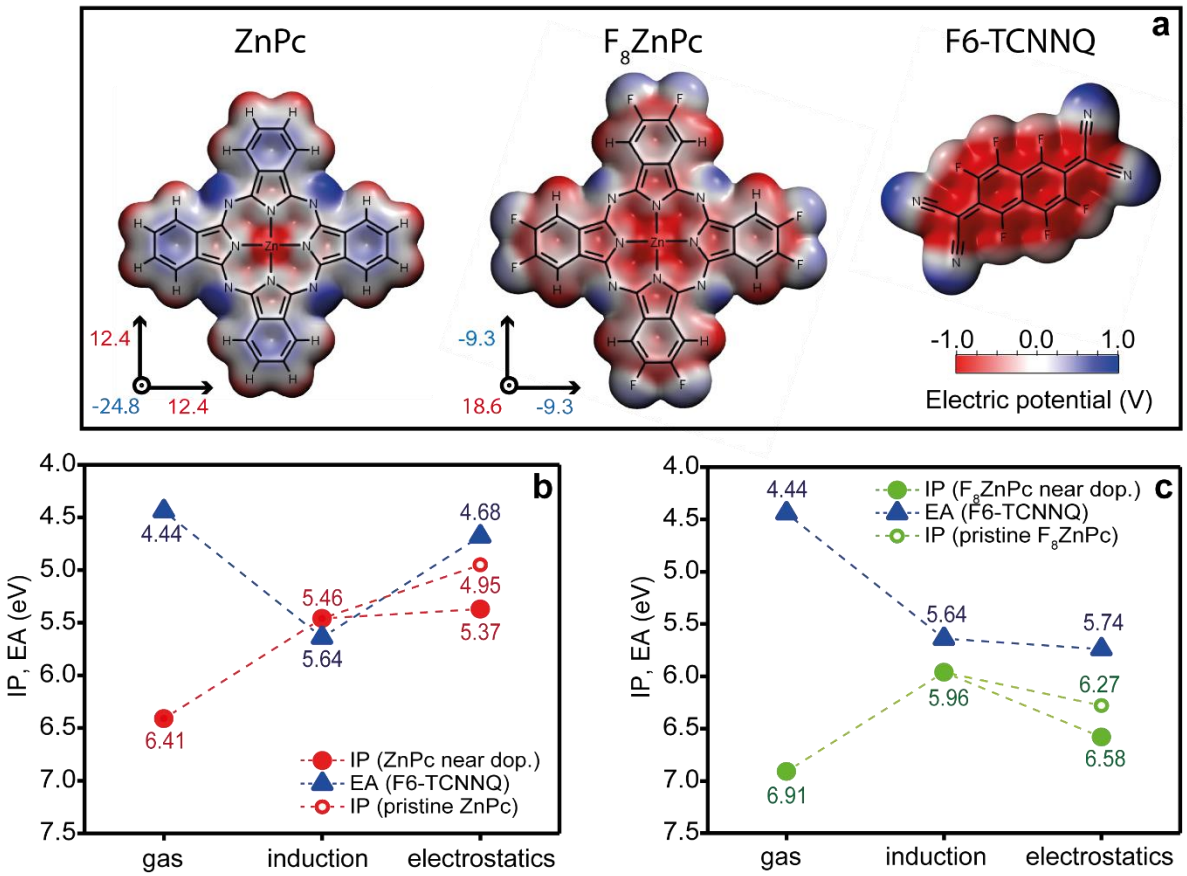

Figure 1. (a) Molecular structures and electrostatic properties (electrostatic potential color maps and molecular quadrupole components expressed in Debye-Å) of ZnPc, F_8ZnPc and F6-TCNNQ, as obtained from DFT calculations at the PBE0/cc-pVTZ level of theory. (b, c) Effect of induction and electrostatic interactions on the frontier energy levels of the dopant (blue triangles) and the host molecules, either next to the dopant (full circle) or in the pristine film (open circle). Specifically, (b) binary blend composed of ZnPc (host, red dots) and F6-TCNNQ (dopant, blue triangles) and (c) binary blend composed of F_8ZnPc (host, green dots) and F6-TCNNQ (dopant, blue triangles). Energy levels are referred to a common vacuum level.

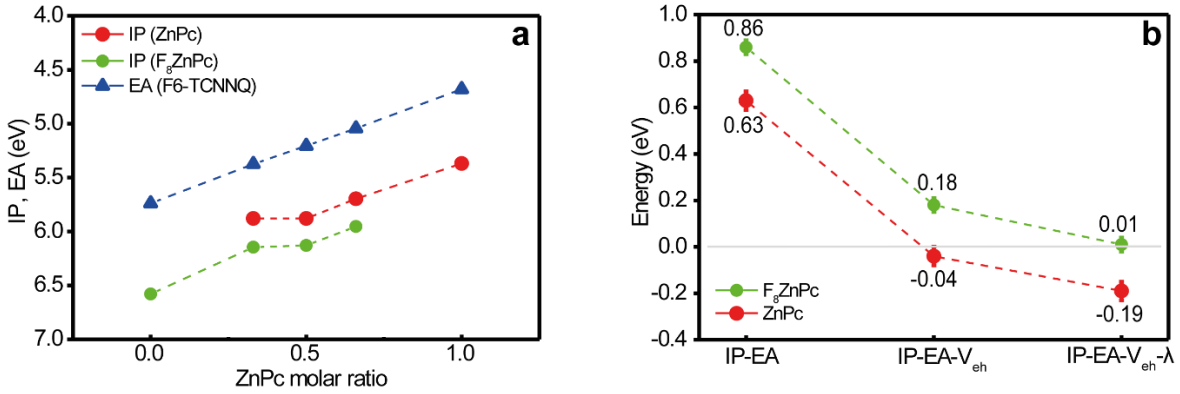

Figure 2. (a) Effect of the solid-state interactions on the IPs of ZnPc (red circles) and F_8ZnPc (green circles) and the EA of F6-TCNNQ (blue triangles) in ZnPc:F8ZnPc blends doped with F6-TCNNQ as a function of ZnPc molar ratio. The data correspond to averages over different microscopic hosts-dopant configurations. (b) Energies of the CT state where the electron is localized on the F6-TCNNQ and the hole either on the nearest-neighbour ZnPc or F_8ZnPc. The energy was calculated by considering different contributions, namely (1) the Γ_{hd} energy difference, (2) the e-h Coulomb interaction (V_{eh}), and (3) the relaxation energy of the CT state (λ). The last two contributions stabilize the Γ_{hd} energy difference and make the CT state more stable.

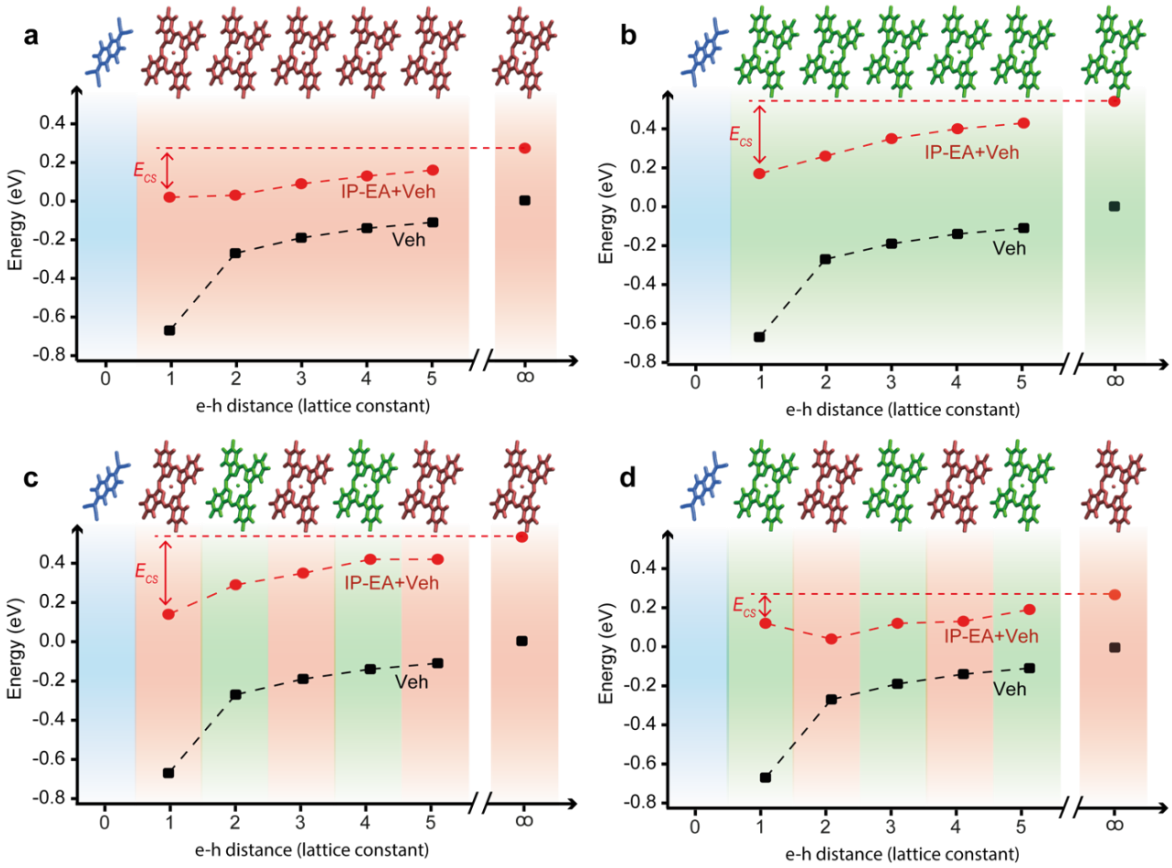

Figure 3. Energies of CT states (red dots), with the electron localized on the F6-TCNNQ and the hole on host molecules, as a function of the electron-hole distance along the π stacking direction. The screened Coulomb binding energies, $V_{eh}(r_{eh})$ (black squares) and the energy barrier for charge separation (E_{cs}) are also shown. The calculations are reported for (a) ZnPc:F6-TCNNQ and (b) F_8ZnPc:F6-TCNNQ binary blends, and two 1:1 configurations of (c,d) ZnPc:F_8ZnPc:F6-TCNNQ ternary blends. These results highlight the striking dependence of the charge separation energy profile on the morphology and composition of the host material.

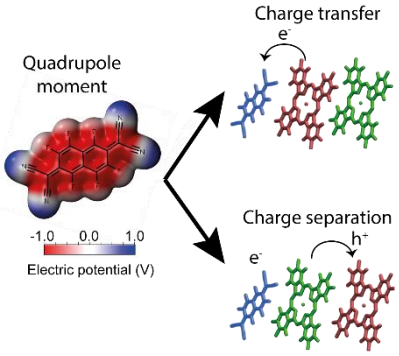

Our micro-electrostatic calculations demonstrate that molecular quadrupole moments of host and dopant molecules fundamentally affect molecular doping of organic semiconductors. Namely, both the dopant ionization and the charge dissociation steps are facilitated by the rearrangement of the frontier energy levels of the host/dopant molecules due to the microscopic electrostatic interactions.

Keyword Molecular doping

Alberto Privitera,[±] Giacomo Londi,[±] Moritz Riede, Gabriele D'Avino, David Beljonne*
±These authors contributed equally

Molecular quadrupole moments promote ground-state charge generation in doped organic semiconductors